CHEMISTRY

Direct visualization of cooperative adsorption of a string-like molecule onto a solid

Yuma Morimitsu[1], Hisao Matsuno[1,2]*, Yukari Oda[3], Satoru Yamamoto[2], Keiji Tanaka[1,2]*

Natural systems, composite materials, and thin-film devices adsorb macromolecules in different phases onto their surfaces. In general, polymer chains form interfacial layers where their aggregation states and thermal molecular motions differ from the bulk. Here, we visualize well-defined double-stranded DNAs (dsDNAs) using atomic force microscopy and molecular dynamics simulations to clarify the adsorption mechanism of polymer chains onto solid surfaces. Initially, short and long dsDNAs are individually and cooperatively adsorbed, respectively. Cooperative adsorption involves intertwining of multiple chains. The dependence of adsorption on the chain affects the formation of the interfacial layer, realizing different mechanical properties of DNA/filler bulk composites. These findings will contribute to the development of light and durable polymer composites and films for various industrial, biomedical, and environmental applications.

INTRODUCTION

Many natural systems for homeostasis of life involve the adsorption of biomacromolecules such as proteins or nucleic acids onto a solid interface (*1*, *2*). For example, prokaryotic cells with a micrometer-scale confined space adsorb DNA, which has a length of tens of micrometers, on the inner surface of lipid membranes (*3*, *4*). In addition, macromolecular adsorption on the interface has been discussed over the last several decades in polymer engineering fields (*5*–*8*). The polymer layer adjacent to a solid surface has a distinct structure from that of the bulk. Their aggregation states (*9*, *10*) and thermal molecular motion (*11*, *12*) completely differ from those in the bulk and are critical factors for the performance of polymer composites (*13*–*15*) and thin-film devices (*16*).

The physisorption of polymer chains from a solution system provides a facile and versatile method to adsorb macromolecules on a surface. Examples include solvent-casting as well as dip- and spin-coating methods. The large internal degree of freedom of each polymer chain makes molecular events behind these experimental procedures complex compared to rigid low–molecular weight compounds with a restricted rotation of internal C—C bonds. Consequently, a single chain has both adsorbed and unadsorbed segments.

Theoretical (*5*, *6*, *17*, *18*) and experimental (*7*–*12*, *19*, *20*) studies have led to the train-loop-tail model. This model describes a chain adsorbed on a solid surface that eventually forms an interfacial layer that is thinner than the dimension of an unperturbed chain. Recent interface-selective spectroscopic studies strongly support this model in terms of the local conformation of chains adsorbed on the surface (*19*, *20*). However, it is unclear whether the whole chain is adsorbed on the surface and contributes to the formation of the interfacial layer.

Here, we directly visualize three double-stranded DNAs (dsDNAs) with different lengths and an almost monodispersed length distribution using atomic force microscopy (AFM). The longest one is an intact λ-phage DNA with 48,490 base pairs (bp) (*21*). The other two are enzyme-digested λ-phage DNAs (fig. S1). Hereafter, these are referred to as DNA48kbp, DNA24kbp, and DNA12kbp, respectively. DNA48kbp has a fully extended chain length (L_{ex}) of 16.5 μm as determined by a calculation that considers the distance between base pairs of the typical B-form conformation (0.34 nm) (*22*). Hepes–sodium hydroxide (NaOH) buffer solutions containing $NiCl_2$, which is referred to *X*Ni, where *X* indicates *X* mM $NiCl_2$, are used to prepare the dsDNA solutions. The persistence length (L_p) of dsDNA in 5Ni estimated by the Netz-Orland theory is 54.3 nm (*23*). Table S1 summarizes other characteristics such as the radius of gyration (R_g) based on the standard worm-like chain model (*24*) and the overlap concentration (C^*).

To date, various biomacromolecules such as dsDNA (*25*–*27*) and proteins (*28*) have been visualized with AFM (*29*). Recent ultrahigh-resolution imaging for single dsDNA molecules such as supercoiled closed circular plasmid DNAs and synthetic oligonucleotides has made it possible to discuss the helical pitch and the winding direction of dsDNA chains as functions of their conformation such as the B- and Z-forms (*25*–*27*). However, information about the adsorption behavior of string-like molecules from a solution to a solid surface is limited. Unlike previous studies, we directly observed the adsorption behavior, and our findings should contribute to a better understanding of their behavior.

RESULTS

Initial adsorption of dsDNA chains

Single molecules were directly visualized to reveal the extension of dsDNA on a solid. Figure 1A shows the AFM height images for dsDNAs with different lengths adsorbed on a mica substrate at concentrations much lower than C^*. String-like molecules with a height of approximately 2 nm, which correspond to the dsDNA diameter, were observed. The contour lengths (L_c's) of individual strings of DNA12kbp, DNA24kbp, and DNA48kbp were 4.0, 8.1, and 15.3 μm, respectively. Figure 1B shows the relationship between the average L_{ex} and L_c. The L_c values were slightly shorter than the corresponding L_{ex} values for all chain lengths. The L_c values were roughly 89 to 94% of the L_{ex} values, suggesting the presence of unadsorbed segments such as loops or tails (*5*, *6*, *30*).

[1]Department of Applied Chemistry, Kyushu University, 744 Motooka, Nishi-ku, Fukuoka, 819-0395, Japan. [2]Center for Polymer Interface and Molecular Adhesion Science, Kyushu University, 744 Motooka, Nishi-ku, Fukuoka, 819-0395, Japan. [3]Division of Applied Chemistry and Biochemical Engineering, Shizuoka University, 3-5-1 Johoku, Naka-ku, Hamamatsu, Shizuoka 432-8561, Japan.
*Corresponding author. Email: h-matsuno@cstf.kyushu-u.ac.jp (H.M.); k-tanaka@cstf.kyushu-u.ac.jp (K.T.)

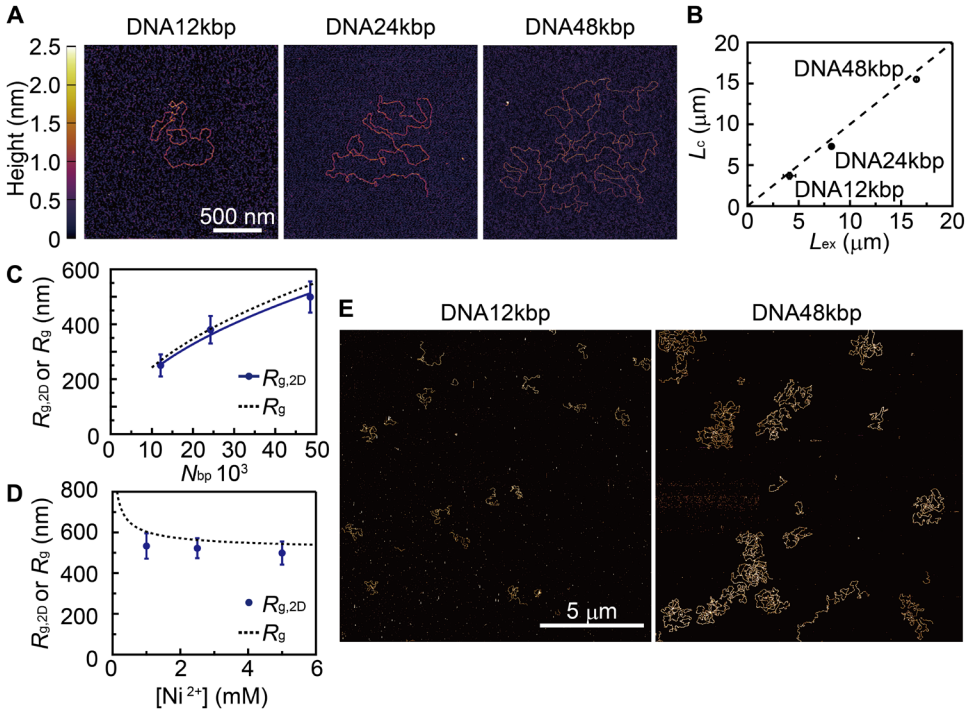

Fig. 1. Effect of chain length on adsorption. (**A**) AFM-based single-molecule imaging for DNA12kbp, DNA24kbp, and DNA48kbp on mica substrates observed in 10Ni. Images were acquired after incubating the mica substrates with 3.1 pM dsDNA solution in 5Ni for 2 min. (**B**) Relationship between L_c and L_{ex}. Dashed line indicates a match between L_c and L_{ex}. (**C**) Plots show the relationship between N_{bp} and $R_{g,2D}$. The blue line corresponds to the best fit of the experimental data assuming $L_{p,2D}$ of 48 ± 7 nm. For comparison, dashed line superimposes R_g in 5Ni. (**D**) [Ni^{2+}] dependence of $R_{g,2D}$ for DNA48kbp. For comparison, the dotted line superimposes R_g in 5Ni. (**E**) AFM images for DNA12kbp and DNA48kbp acquired under the same condition as those for (A), except the incubation time was increased to 30 min.

This study examined the chain dimension of dsDNA chains adsorbed from a solution onto a solid. That is, chains were sandwiched between a hard wall and liquid molecules, where one side of the chain was in contact with the solid substrate and the other was in contact with a solution. Because segments of adsorbed chains in the liquid phase play an important role in the successive adsorption, this study is of pivotal importance. Figure 1C shows the two-dimensional (2D) R_g on mica ($R_{g,2D}$) obtained by tracing the chain trajectory in AFM images (see details in the "AFM observations and analyses" section and in fig. S2) as a function of base pairs (N_{bp}). The $R_{g,2D}$ increased with increasing N_{bp}. Each $R_{g,2D}$ agrees well with the corresponding R_g in 5Ni. A solid curve was the best fit based on the worm-like chain model assuming a persistence length in 2D ($L_{p,2D}$) of 48 ± 7 nm. This observation is consistent with L_p in 5Ni (54.3 nm).

In addition, it has been reported that the interaction between dsDNA and mica depends on [Ni^{2+}] (*31*). Figure 1D shows the ionic strength effect on $R_{g,2D}$'s. The $R_{g,2D}$ values at three different [Ni^{2+}] were almost identical. Thus, the ionic strength is not a dominant factor for the conformation of adsorbed chains within the [Ni^{2+}] region used.

The AFM scan area was enlarged, and image processing (see details in the "AFM observations and analyses" section) was performed to evaluate the impact of chain length on adsorption. Figure 1E shows wide-area images of DNA12kbp and DNA48kbp acquired after incubating for 30 min. DNA12kbp chains were independently adsorbed. That is, overlap was not observed. Hereafter, this is defined as isolated adsorption, which is similar to Langmuir-type adsorption where the adsorbates do not interact. In addition to isolated adsorption, DNA48kbp chains adsorbed in adjoining or contact states with other chains. This was also the case for DNA24kbp (fig. S3). Note that adsorption following this manner occurred although the solid contained a lot of empty areal spaces. Thus, other chains, which were preadsorbed and formed looped structures on mica, affected the adsorption of longer chains. Hereafter, this is referred to as cooperative adsorption. Cooperative adsorption involving multiple chains should occur more easily for longer chains.

The influence of the incubation time on DNA48kbp samples was also evaluated on the basis of reciprocal- and real-space methods using fast Fourier transform (FFT) and circumscribed circles, respectively. Figure 2A represents AFM images for DNA48kbp chains adsorbed on mica acquired in 10Ni after incubating in 3.1 pM solution for 2, 5, 10, 20, and 30 min. The amount of adsorbed chains increased with increasing incubation time, and something like a domain was formed. For the 2-min incubation, two DNA48kbp chains were observed in the 25 μm–by–25 μm area. Figure 2B shows the average FFT power spectrum obtained from six AFM images acquired under the same conditions. Because DNA48kbp chains observed at 2 min were adsorbed in an independent manner and not a cooperative one, the spectrum can be taken as a form factor (*32*). Figure 2B shows the spectra obtained at various incubation times divided by the form factor (*33*, *34*). These spectra correspond to the structure factors. At 5 min, a prominent peak was confirmed at $L^{-1} = 6.7 \times 10^{-4}$ nm^{-1}. The L^{-1} value corresponds to the length scale of 1.5 μm, which is approximately three times larger than $R_{g,2D}$ of DNA48kbp shown in Fig. 1C. Given that the domains were composed of two or more adsorbed dsDNA chains due to cooperative adsorption, the characteristic length of 1.5 μm

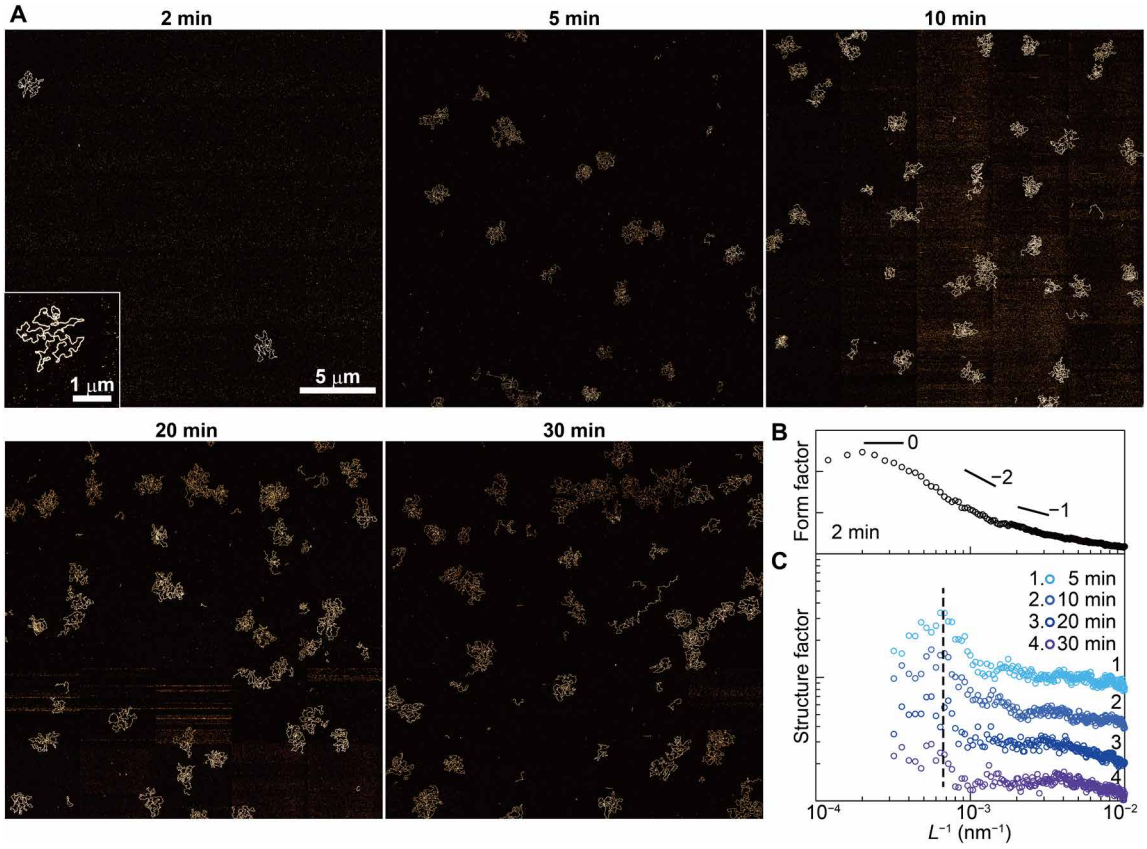

Fig. 2. Cooperative adsorption of dsDNA. (**A**) AFM images for DNA48kbp adsorbed on mica acquired in 10Ni after incubating with a 3.1 pM DNA48kbp solution in 5Ni for 2, 5, 10, 20, and 30 min at 304 K. Inset is an enlarged image. (**B**) Average FFT power spectrum obtained from six AFM images acquired after incubating for 2 min. This spectrum was used as the form factor (*32*). (**C**) Spectra of the structure factor obtained by dividing the FFT spectra for 5 to 30 min by the form factor (*33*, *34*). Peak around 6.7×10^{-4} nm^{-1} corresponds to the distance between the adsorbed dsDNA chains on mica. The calculated value is 1.5 μm.

should be the distance between dsDNA chains in the domain on mica. Note that the incubation time did not influence the position of the peak corresponding to the structure factor. These results demonstrate that DNA48kbp chains tended to cooperatively adsorb onto mica with other chains.

Alternatively, real-space analysis using circumscribed spheres was conducted (fig. S4). Each DNA48kbp chain was surrounded by a blue circle (fig. S4A). Then, the distance among the centers of each circle was estimated. From the histogram shown in fig. S4B, the highest population occurred at a distance from 1 to 2 μm, regardless of the incubation time. The distance is comparable to the characteristic length of 1.5 μm obtained by FFT analysis. In addition, the broad distance distribution beyond 2 μm corresponds to the distance between domains. These results confirm that cooperative adsorption of DNA48kbp chains occurs on mica.

Next, the mechanism of cooperative adsorption was investigated. Figure 3A shows dsDNA chains adsorbed at a lower ionic strength (3Ni) weakened the interaction between dsDNA chains and mica. It is plausible that ca. 65% of a whole chain remains as movable segments in the liquid phase like a loop structure (*5*, *6*, *30*) because L_c of 5.9 μm for DNA48kbp was much shorter than L_{ex}. In addition, an unclear clipped white region (yellow arrow) due to trapping by the AFM tip upon scanning was observed. These partially adsorbed chains were in an intermediate state during the adsorption process, and some segments sought adsorption sites on the solid.

Figure 3B shows an AFM image of two dsDNA chains intertwined on mica after incubating with 3.1 pM DNA48kbp solution in 5Ni for 5 min. This intermolecular intertwining should form only near the surface because the concentration was much lower than C^*. Thus, it can be regarded as a transient entanglement (*35*). Cooperative adsorption was more common than isolated adsorption (see Fig. 1E). This is probably because a partially adsorbed chain captures a free chain via intertwining, leading to enforced adsorption of a chain onto the solid. That is, cooperative adsorption is due to many loop and tail segments, yielding a highly interactive interface with other free dsDNA chains via intertwining, as described later.

Figure 3C summarizes the macromolecular picture for the initial adsorption onto the solid surface. (1) A chain is partially adsorbed. Then, the chain is either (2′) adsorbed on the solid (isolated adsorption) or (2) captured by a free chain via intertwining, which leads to (3) successive adsorption of the captured chain (cooperative adsorption). In the latter case, multiple chains become intertwined and are adsorbed to the solid. This behavior completely differs from the well-established Langmuir-type adsorption, which is observed in low–molecular weight compounds.

Formation of the interfacial layer

Next, the formation of the interfacial layer on a solid was evaluated. Figure 4A shows AFM images for specimens after incubating with

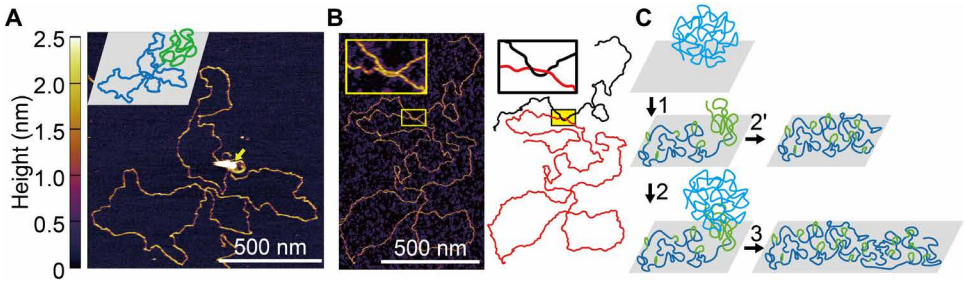

Fig. 3. Macromolecular picture of initial adsorption. (**A**) AFM image for DNA48kbp observed in 3Ni after incubating mica with 3.1 pM DNA48kbp solution in 3Ni for 2 min. Inset: Illustration of a dsDNA chain, where blue and green show real and imaginary segments, respectively, depicted from the main panel. (**B**) Left: AFM image for two DNA48kbp chains observed in 10Ni after incubating with a 3.1 pM solution in 5Ni for 5 min. Right: For clarity, black and red lines schematically depict the strings. Inset: Enlarged view of two intertwined dsDNA chains. (**C**) Depiction of adsorption. Free chain in a solution (light blue) is (1) partially adsorbed followed by (2′) isolated adsorption on a solid or (2) the intertwinement with other free chains, which leads to (3) cooperative adsorption.

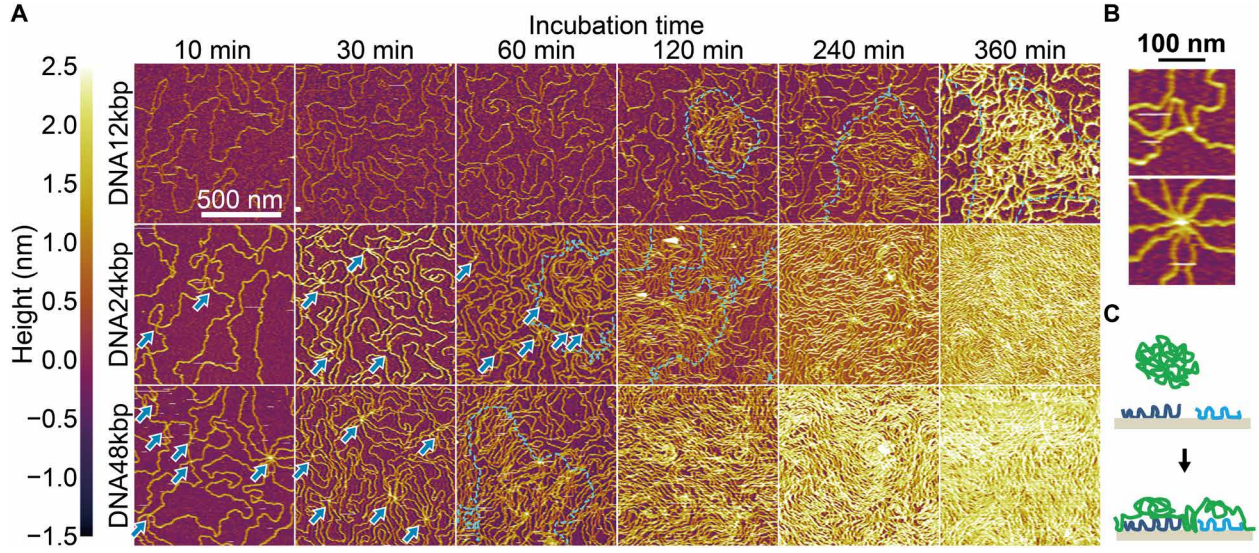

Fig. 4. Formation of interfacial layers. (**A**) AFM images for three kinds of dsDNA chains acquired after incubating mica substrates with 62.5 pM dsDNA solution in 2.5Ni for 10 to 360 min and subsequently washing with water. (Top) DNA12kbp, (middle) DNA24kbp, and (bottom) DNA48kbp. (**B**) Enlarged images for (top) DNA24kbp and (bottom) DNA48kbp to clarify the overlapping points. Images were acquired after incubating for 10 min. (**C**) Schematic illustration of the proposed bridging adsorption.

62.5 pM dsDNA solution in 2.5Ni for different times and subsequently washing with water. The amount of adsorbed chains for DNA24kbp increased with the incubation time (Fig. 4A, middle). Between 10 and 60 min, the mica substrate was covered by chains with many overlapping points (blue arrows) due to cooperative adsorption. Figure 4B (top) shows an enlarged view at 10 min to clarify the overlapping points. The chain density increased as the time increased from 120 to 240 min. Aggregates in which the chains piled up or intertwined formed (blue dashed lines), and the aggregate size dimension increased. A similar adsorption behavior was observed for DNA48kbp, as shown in Fig. 4A (bottom) and Fig. 4B (bottom). Figure 3B shows that intertwining occurs in the case of longer DNA48kbp even at a lower concentration (3.1 pM). Hence, it seems reasonable that many overlapping points formed at a higher concentration. These results suggest successive adsorption of chains bridging over chains, which were already adsorbed. That is, "bridging" adsorption occurs due to insufficient unoccupied sites (Fig. 4C).

Then, the occurrence of cooperative adsorption of DNA12kbp onto the surface was examined. Initially, the number of adsorbed chains increased with negligible overlapping regions because isolated adsorption was dominant (Fig. 4A, top). The areal density of chains after 120 min was much lower than DNA24kbp and DNA48kbp. This was because the bridging adsorption hardly occurred for shorter chains such as DNA12kbp. However, aggregates started to form at 120 min. Even for DNA12kbp, some partially adsorbed chains contributed to the capture of free chains, leading to mass adsorption by sharing anchoring points. However, 14 hours were necessary to completely cover the surface because the probability of cooperative adsorption was low for shorter chains (fig. S5).

The amount of dsDNA adsorbed on mica was quantitatively analyzed. Figure 5 (A and B) shows the surface coverage and adsorption amount of dsDNA as functions of incubation time, respectively. For DNA24kbp and DNA48kbp, the surface coverage increased relatively quickly with incubation time and eventually reached unity. On the other hand, the increase in surface coverage was gradual for

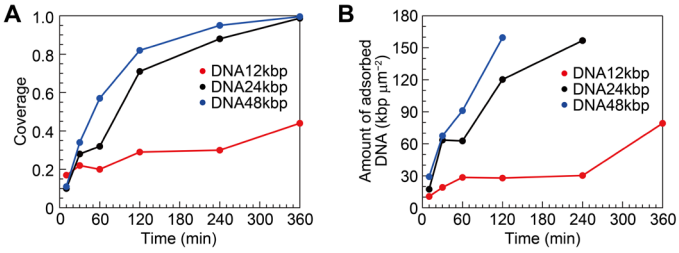

Fig. 5. Surface coverage and amount of DNA for interfacial layers. (**A**) Surface coverage and (**B**) amount of DNA as functions of incubation time estimated from the AFM images shown in Fig. 4A.

DNA12kbp. Because the difference in the surface coverage between DNA24kbp and DNA48kbp was small, it is likely that there is a threshold where cooperative adsorption becomes dominant between DNA12kbp and DNA24kbp. In addition, a similar length effect was observed for the amount of adsorbed dsDNA (Fig. 5B). However, the value at a high coverage was not obtained because AFM could not access the mica surface to quantify the height of adsorbed dsDNA chains.

Next, the amount of dsDNA adsorbed on the mica surface and the amount of dsDNA floating in the buffer solution under the conditions used were estimated. For example, the adsorbed amount of 160 kbp μm^{-2}, which is the apparent asymptotic value for DNA24kbp in Fig. 5B, is equivalent to approximately 7 chains μm^{-2}. Similarly, 160 kbp μm^{-2} corresponds to 13 and 3 chains μm^{-2} for DNA12kbp and DNA48kbp, respectively. In contrast, on the basis of the concentration of each dsDNA solution mounted on mica, dsDNA chains floating in the solution on the mica surface before adsorption were estimated to be approximately 3211 kbp μm^{-2}. This value, which is given per unit area rather than the volume, corresponds to approximately 268, 134, and 67 chains μm^{-2} for DNA12kbp, DNA24kbp, and DNA48kbp, respectively. In the case of shorter DNA12kbp, the amount of adsorbed chains could not reach the apparent asymptotic value for other dsDNA chains, 160 kbp μm^{-2}, even after 360 min. The difference in the amount of adsorbed chains among the three kinds of dsDNAs became remarkable over time, suggesting that the adsorption of string-like molecules to the solid surface becomes faster as cooperative adsorption occurs.

The above hypothesis for chain adsorption was verified by coarse-grained molecular dynamics (CGMD) simulations (*36*). The simulations confirmed cooperative adsorption for longer chains and the aforementioned bridging adsorption. Figure 6A shows snapshots of adsorbed chains at 65% surface coverage, where each color indicates a different chain. Although most shorter chains, which consisted of 10 particles, were firmly adsorbed on the substrate, a short chain formed a tail structure (Fig. 6A, bottom left). However, the intertwining of the tail segment with other free chains was not discerned because of the short length as the incubation time increased. On the other hand, longer chains, consisting of 40 particles, were partly adsorbed, and the rest swayed on the solvent side. Figure 6B illustrates the cooperative adsorption process observed in the simulation. The blue adsorbed chain (black arrow) interacted with, or was stuck on, a light blue chain in the solvent (a). The light blue chain was subsequently attracted to the substrate side (b) and eventually adsorbed on it (c and d). Simultaneously, the bridging adsorption proposed in Fig. 4C was also observed.

Composite properties tuned by the interfacial layer

The influence of the aggregation states of the interfacial layer on the mechanical properties of composite materials was finally assessed. A model of bulk films composed of DNA and hydrated choline dihydrogen phosphate (CDP) with a feed ratio of DNA/CDP [60/40 (w/w)] (DC40), which were rubbery-like at room temperature, was used (*37*). Silica (SiO_2) particles adsorbed with short DNA (S-DNA) (approximately 0.9 kbp) and long DNA (L-DNA) (48 kbp), which are referred to as SiS and SiL particles, respectively, were used as fillers (see figs. S6 and S7 and more discussion in text S1). While SiL particles aggregated in water, SiS particles were well dispersed, as evidenced by optical microscopy (fig. S8A). This means that the loop and tail segments (*6*) existed in the interfacial layer of SiL, as a result of longer chains adsorbed in the cooperative and bridging manner. These segments intertwined with those on other particles for SiL. On the other hand, SiS particles had less interaction with other particles due to fewer loop and tail segments, resulting from shorter chains adsorbed independently. DC40 films containing SiS or SiL particles with a 5% SiO_2 weight ratio (W_{Si}), which are referred to as DC40S5 and DC40L5, respectively, were prepared [see fig. S8 (B and C) and more discussion in text S1].

Figure S9A shows the shear strain (γ) dependence of complex shear modulus (G^*) for the composite films. The composite films had a higher G^* value than that for the DC40 film within the linear viscoelastic regime due to the presence of SiO_2. G^* slightly decreased with increasing γ and started to decrease after 2.5 and 6.3% for the DC40S5 and DC40L5 films, respectively. Repeating the measurement right after the first run essentially yielded the same results. Figure S9B shows the stress (σ)–strain (ε) curves for the DC40S5 and DC40L5 films. Young's modulus estimated based on the initial slope of the curves was approximately 40 MPa and was independent of the length of chains adsorbed onto SiO_2 particles. The yield stresses were also comparable to each other. On the other hand, the break point was greater for DC40L5 than for DC40S5. Table S2 summarizes the parameters for the tensile properties.

DISCUSSION

The AFM imaging for dsDNA chains adsorbed on mica revealed that the $R_{g,2D}$ was in good accordance with the corresponding R_g in a solution state (Fig. 1C). However, this finding appears to be inconsistent with published results for dsDNA chains confined in 2D space using slit-like channels, which depend on the gap thickness or the extent of the confinement (*38*–*40*). dsDNA chains in a solution state confined between less interactive slits are swollen, and R_g is, at most, double the original one.

Under the current experimental condition, a dsDNA chain exists freely in the solution at the beginning. Then, a segment of a chain starts to interact with a solid surface, resulting in a partially adsorbed segment. At this point, the locally adsorbed segment loses its mobility, which means that it does not collide with other segments. That is, the other segments in the vicinity of the segment are unaffected by the excluded volume from the preadsorbed segment. Thus, the successive adsorption of segments proceeds under a similar excluded volume effect in solution. In addition, the solution concentration of dsDNA is much lower than the C^*. Thus, the amplification of the excluded volume effect becomes insignificant. That is, the scaling law regarding the worm-like chain model established

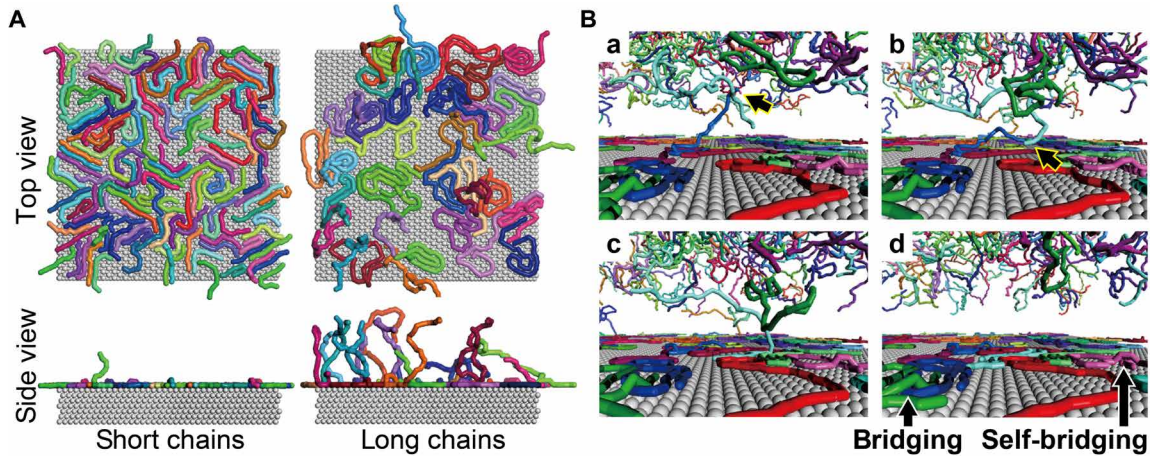

Fig. 6. Snapshots of chain adsorption by CGMD simulations. (**A**) Top and side views of adsorbed chains for the short- and long-chain systems with a surface coverage of 65%. (**B**) Characteristic scenes of cooperative adsorption observed in the long-chain system. Bridging adsorption also occurs.

for 3D polymer chains in solution or melt states may be applicable to 2D chains adsorbed on the solid surface (*41*).

Next, the universality of cooperative adsorption was considered. In the case of dsDNA, the threshold length at which the adsorption mechanism changes from an independent to a cooperative one falls between DNA12kbp and DNA24kbp. Because the L_p value for dsDNA was approximately 54 nm and the typical distance between base pairs was 0.34 nm (*22*, *23*), the estimated L_{ex} values for DNA12kbp and DNA24kbp were approximately 76 L_p (= 12.121 [kbp] × 0.34 [nm/bp]/54 [nm/L_p]) and 152 L_p, respectively. That is, the threshold L_{ex} value should be located between 76 L_p and 152 L_p. The molecular structure of polystyrene (PS) chains adsorbed on a silicon wafer, which is one of the most studied systems, was well characterized (*42*). In the case of a mass-average molar mass ($\bar{M}_w$) smaller than 50 kg mol^{-1}, a PS film is unstable because dewetting occurs at a temperature above the bulk glass transition temperature (T_g). This was not the case for a high-$\bar{M}_w$ PS film ($\bar{M}_w \geq$ 123 kg mol$_{-1}$).

These results can be explained in terms of the local conformation. Longer chains formed many loops, which prevented dewetting, whereas shorter chains preferred to form trains. Considering that the L_p value of PS was approximately 1.0 nm (*43*), the length of two adjacent repeating units was 0.25 nm, the polydispersity index of PSs used was less than 1.15, and the molecular weight of a styrene unit was 104; the L_{ex} values of PSs with $\bar{M}_w$'s of 50 and 123 kg mol^{-1} were roughly estimated to be 105 L_p (= {50 × 10$_3$/(1.15 × 104)} [U] × 0.25 [nm/U]/1.0 [nm/L_p]) and 257 L_p. Thus, a conformational transition from a train to loop one likely occurs in the range from 105 L_p to 257 L_p. Although the threshold L_{ex} value for the conformational transition and consequently the adsorption mechanism of PS was roughly estimated, it agrees with that for dsDNA mentioned above.

The adsorption behavior of poly(methyl methacrylate) (PMMA) chains onto mica (*44*) was also discussed. PMMA chains with $\bar{M}_w$'s of 30.5 and 315 kg mol^{-1} were independently and cooperatively adsorbed on mica, respectively. The reported L_p value of PMMA was approximately 1.3 nm (*45*). L_{ex} values of PMMAs with $\bar{M}_w$'s of 30.5 and 315 kg mol^{-1} were 54 L_p and 577 L_p, implying that the conformational transition from more trains to more loops occurs between 54 L_p and 577 L_p. Therefore, in the case of synthetic polymers, longer chains were likely adsorbed on the solid surface with many loop and tail conformations, resulting in cooperative and bridging adsorption.

The reduction of G^* as γ increases shown in fig. S9A is often observed for rubber composites. This is known as the Payne effect and can be explained in terms of the deformation and the breaking of the filler network (*46*). However, even after γ increased to 100%, at which G^* became approximately one order smaller, G^* completely recovered to the original value at a smaller γ. Thus, the effect of the filler network on the γ versus G^* relationship should be negligible. The difference in the threshold γ between DC40S5 and DC40L5 in fig. S9A is attributed to the difference of the aggregation states of chains at the filler interface. That is, it is due to the presence or absence of intertwining chains at the interface. Similar results were observed on the σ–ε curves (fig. S9B). The break point for DC40L5 was greater than that for DC40S5, indicating that DC40L5 had a larger energy barrier for flowing DNA chains. This can be explained in terms of the existence of looped and tailed segments on SiO_2 surfaces, which prevented DNA chains from flowing due to intertwining.

In conclusion, AFM-based direct visualization reveals that the dimension of polymer chains adsorbed on a surface is comparable to that in the solution state. CGMD simulations reveal that, unlike small molecules, which adsorb in an isolated manner consistent with Langmuir's hypothesis, polymer chains adsorb on the surface in both isolated and cooperative manners. Longer chains predominantly undergo cooperative and successive bridging adsorptions to form an interfacial layer on the solid surface. In contrast, shorter chains undergo isolated adsorption and cooperative adsorption is rare. Partially adsorbed shorter chains slowly form an interfacial layer. These adsorption manners affect the macroscopic mechanical properties of the composites. The interfacial layer formed from longer chains induces flexible filler networks compared with shorter chains. Our study using a narrow dispersion of dsDNAs provides a comprehensive understanding of the macromolecular picture. The results should be useful to design interfacial layers and to develop polymer-based composite materials for applications in various industrial, environmental, and biomedical fields.

MATERIALS AND METHODS

Materials

λ-DNA dissolved in a buffer solution of 10 mM tris–hydrochloric acid (tris-HCl; pH 7.9) containing 1 mM EDTA was purchased

from Nippon Gene (Tokyo, Japan). The concentration of λ-DNA was 0.54 μg/μl (lot no. 40047E). Hepes, $NiCl_2 \cdot 6H_2O$, 6 M HCl, and ethanol were purchased from FUJIFILM Wako Pure Chemical (Osaka, Japan). NaOH was purchased from Kanto Chemical (Tokyo, Japan). Tris was purchased from Kishida Chemical (Osaka, Japan). An EDTA disodium salt dihydrate was purchased from Junsei Chemical (Tokyo, Japan). A phenol-chloroform-isoamyl alcohol (PCI) mixture was purchased from Merck (Darmstadt, Germany). For bulk composite samples, a suspension of amine-functionalized SiO_2 particles with diameters of approximately 3 μm (50 mg/ml) was purchased from Micromod Partikeltechnologie (Rostock, Germany). Powdered DNA sodium salt (approximately 0.9 kbp) purified from salmon and herring sperm was purchased from MP Biomedicals (Santa Ana, CA, USA). CDP was purchased from Kanto Chemical (Tokyo, Japan). Restriction enzymes Pvu I–HF and Xba I were purchased from New England Biolabs (NEB; Ipswich, MA, USA). All reagents were analytical grade and used as received without further purification.

Ultrapure water was prepared using a Milli-Q system (Merck). As a standard buffer solution, 1 M Hepes-NaOH (pH 6.8) was prepared according to the standard protocol. An aqueous solution of $NiCl_2$ at 1 M was also prepared. Both solutions and ultrapure water were mixed at predetermined ratios to prepare 40 mM Hepes-NaOH containing *X* mM $NiCl_2$ (*X*Ni). In addition, 10 mM tris-HCl (pH 8.0) containing 1 mM EDTA (TE) was prepared.

Preparation of the dsDNA solutions

DNA48kbp

A λ-DNA solution was diluted by TE. The concentration of the dsDNA stock solution was confirmed on the basis of "ultraviolet-visible (UV-Vis) spectroscopy" using a UV-Vis-NIR spectrometer (Hitachi High-Tech Science, Tokyo, Japan). The concentration was 6.0 μg/ml.

DNA24kbp

λ-DNA was digested using restriction enzyme Xba I according to the following procedure. λ-DNA (2 μg), 20 U of Xba I, and 5 μl of 10X CutSmart buffer were mixed. Then, ultrapure water was added to increase the total volume up to 50 μl. The mixture was incubated at 310 K for 1 hour. Last, the product was extracted and purified by standard PCI extraction and ethanol precipitation methods. The concentration of dsDNA in TE was 3.0 μg/ml.

DNA12kbp

λ-DNA was digested using restriction enzyme Pvu I in a similar manner as above. λ-DNA (2 μg), 20 U of Pvu I–HF, and 5 μl of 10X CutSmart buffer were mixed. Then, ultrapure water was added to increase the total volume up to 50 μl. The mixture was incubated at 310 K for 1 hour. Last, the product was purified using a NucleoSpin Gel and PCR Clean-up kit (MACHEREY-NAGEL, Düren, Germany). The concentration of dsDNA in TE was 1.5 μg/ml. Before use, each stock solution was diluted by *X*Ni at a predetermined concentration.

Calculation of L_p, R_g, and C^*

The L_p of dsDNA was calculated on the basis of Netz-Orland theory (*23*). The dependence of the divalent cation on L_p was considered using the parameters for Mg^{2+} reported in the literature (*47*). This is reasonable because the radii of Ni^{2+} (0.069 nm) (*31*) and Mg^{2+} (0.070 nm) (*47*) are almost the same. The R_g in 5Ni was calculated on the basis of the standard worm-like chain model according to the following equation (*24*)

$$R_g^2 = \frac{1}{3}L_{ex}L_p - L_p^2 + \frac{2L_p^3}{L_{ex}}\left[1 - \frac{L_p}{L_{ex}}\left\{1 - \exp\left(-\frac{L_{ex}}{L_p}\right)\right\}\right] \quad (1)$$

The C^* was calculated as

$$C^* = \frac{M}{N_A} \cdot \frac{3}{4\pi\langle R_g^2\rangle^{3/2}} \quad (2)$$

where M and N_A are the molar mass and Avogadro constant, respectively.

Preparation of AFM samples

As a solid substrate, freshly cleaved mica disks (mica disks highest grade V1; Ted Pella, Redding, CA, USA) were used. They were incubated with 100 μl of a dsDNA solution in 5Ni at 3.1 pM (DNA12kbp, 25 ng/ml; DNA24kbp, 50 ng/ml; and DNA48kbp, 100 ng/ml) for a predetermined time at 304 K and subsequently washed with 10Ni. Each sample was stored in 10Ni before the observation. To observe the intermediate state in the adsorption process, mica disks were incubated with the DNA48kbp solution in 3Ni at 3.1 pM for 2 min. Then, samples were washed with 10Ni and stored in 10Ni before observations.

To observe the interfacial polymer layers, freshly cleaved mica disks were incubated with a dsDNA solution in 2.5Ni at 62.5 pM (DNA12kbp, 0.5 μg/ml; DNA24kbp, 1.0 μg/ml; and DNA48kbp, 2.0 μg/ml) for a predetermined time at room temperature and were subsequently washed with ultrapure water. All samples were stored in 10Ni before observations.

AFM observations and analyses

The morphologies of dsDNA adsorbed on mica were observed by AFM (Cypher ES, Asylum Research, Oxford Instruments, Santa Barbara, CA, USA). AFM measurements were conducted in a 10Ni buffer solution at 304 K using a cantilever (BL-AC40TS-C2, Olympus, Tokyo, Japan) with a spring constant of 0.1 N m^{-1} and a resonant frequency of 20 to 30 kHz. The scan rate was 4.34 Hz with scanning densities of 1536 points per line and 1536 lines per frame. The frame size was either 2 μm by 2 μm or 5 μm by 5 μm. The intermediate state during initial adsorption was observed via AFM measurements in 3Ni. To quantify the amount of adsorbed dsDNA chains, the tip convolution effect was corrected on the basis of the diameter of dsDNA.

The tracing of the chain trajectory was based on a self-coded python module using NumPy (*48*) and OpenCV (*49*) libraries. Figure S2 shows a typical tracing process. First, the kink positions were manually clicked to record them, which enabled tracing of the chain morphology, as marked by the white circles and yellow lines. Then, the spline interpolation was applied to the dataset of positions to determine the position data for certain lengths. Last, $R_{g,2D}$ was calculated using the following equations

$$R_{g,2D^2} = \frac{1}{n+1}\sum_{i=0}^{n}(r_i - r_G)^2 \quad (3)$$

$$r_G = \frac{1}{n}\sum_{i=0}^{n} r_i \quad (4)$$

where r_i refers to the position of data number i and n is the total number of data points in the dataset after spline interpolation.

Python libraries [SciPy (*50*) and OpenCV (*49*)] were used to combine 25 images for 5 μm by 5 μm to obtain a wide-area image of 25 μm by 25 μm with a high resolution. The same python libraries were used for FFT analyses of the AFM images. First, the morphology and aggregation state of dsDNA chains were considered. Salt-and-pepper noise was deleted by setting heights to 0 and 4 nm for pixels observed as less than 0.4 nm and more than 4 nm, respectively. Second, the height contrast was highlighted in FFT analysis by standardizing the height. The maximum and minimum heights were set to image intensities of 255 and 0, respectively. Third, the 25 images (5 μm by 5 μm) were combined into a single wide image (25 μm by 25 μm). Then, using the well-established module "scipy.fftpack.fft2" of the SciPy library, the FFT process was applied to the single wide image.

Real-space analysis using circumscribed spheres was conducted by self-organized python codes using the OpenCV library (*49*) as follows. First, a background subtraction and blurring process was applied to the AFM image, and the contour shape of a dsDNA strand was traced. Second, the well-established module "cv2.findContours" of the OpenCV library was used to draw a circumscribed circle. Third, the formation of an aggregate composed of multichains was judged on the basis of whether both the radius of the circle and the chain coverage within the circle exceeded the optimized threshold. Then, the outline of the aggregate was cut in half at the center of the circumscribed ellipsoid along the minor axis. Then, a circumscribed circle of the contour of the cut aggregate was drawn. The third and fourth steps were repeated until each circle was no longer considered an aggregate.

CGMD simulation

All simulations were performed using the Mesocite module in the Materials Studio 2021 (Dassault Systèmes) software package. The adsorption of polymer chains in the solvent was investigated using a substrate with a size of 20 nm by 20 nm. The polymer chain was represented by connecting 10 or 40 CG particles with a diameter of 0.47 nm, corresponding to four carbon atoms, for shorter and longer chains, respectively. The interactions between particles were expressed using the MARTINI force field (*51*). The solvent was represented using the same particles as those constituting the polymer chain. A virtual face center cubic structure was created for the substrate, and the (111) face was cleaved (*52*). The coordinates of the substrate particles were constrained during the simulation. For the substrate particles, the interaction with the polymer chains was set at three times stronger than that of the solvent in the Lenard-Jones potential. This is consistent with the literature comparing the interaction with all-atom MD simulations (*53*). Initially, 800 and 200 polymer chains were randomly generated with solvent particles to a density of 1.0 g cm^{-3} so that shorter and longer chains had equal molar concentrations. The number of solvent particles was 190,416. A CGMD simulation of 200 ns was performed at 298 K under an NVT ensemble with the Nosé-Hoover-Langevin algorithm for temperature control.

Preparation of DNA-adsorbed SiO_2 particles

Two kinds of DNA solutions were used: S-DNA and L-DNA. The S-DNA solution was prepared by dissolving powder DNA (approximately 0.9 kbp) from salmon and herring sperm in TE at 36 μg/ml. The L-DNA solution was prepared by diluting a λ-DNA solution (48 kbp) using TE. Blend solutions of each DNA and SiO_2 particles were prepared by adding 1 ml of a SiO_2 particle suspension into 10 ml of an S-DNA or L-DNA solution. That is, the final concentration of each DNA was set to 32.7 μg/ml. Each blend solution was stirred at room temperature for 24 hours to complete DNA adsorption onto SiO_2 particle surfaces. The DNA chains were easily adsorbed onto the amine-functionalized surfaces due to the electrostatic interaction. To remove the unadsorbed DNA chains in solution, the solvent in each solution was replaced twice by ultrapure water using the centrifugal separation method at a spinning rate of 11,000 rpm for 10 min, yielding S-DNA– and L-DNA–coated SiO_2 particles in suspension (20 mg/ml). A digital camera recorded the sedimentation behaviors of SiS and SiL in water as functions of time.

Preparation of composite films

An aqueous solution of 1.5 weight % (wt %) of S-DNA or 2 wt % of CDP was prepared by dissolving S-DNA or CDP, respectively, into ultrapure water. Mixtures of S-DNA/SiS and S-DNA/SiL with weight ratios of 95/5 (w/w) were prepared by adding each suspension into an S-DNA solution in an arbitrary ratio at room temperature. The mixtures were cast onto a dish made from tetrafluoroethylene-perfluoroalkylvinylether copolymer after adding a CDP solution with a DNA/CDP weight ratio of 60/40 (w/w). Water was evaporated by storing them at 303 K for 4 days, yielding self-supporting DNA films containing CDP and SiO_2 particles. The thickness of the films was approximately 200 μm. All samples were left in a vacuum oven at room temperature for at least 4 hours to dry uniformly. Then, they sat in a container with a relative humidity of 42% at room temperature for at least 12 hours. In addition, a DC40 film without SiO_2 particles was prepared as a reference.

Estimation of interfacial layer thicknesses of DNA on SiO_2 particles

The amount of DNA chains on SiO_2 particles was determined by thermogravimetric analysis (TGA). The measurements used a TG/DTA7300 system (Hitachi High-Tech Science, Tokyo, Japan) with a heating rate of 10 K min^{-1} ranging from room temperature to 1200 K under a nitrogen purge. Neat SiO_2 particles were prepared by drying a SiO_2 suspension under a standard atmosphere at 313 K overnight. Then, they were placed in an alumina pan.

Chemical composition of the films

The chemical compositions of the films were determined by TGA with a heating rate of 10 K min^{-1} from room temperature to 473 K under a nitrogen purge. Pieces of the films were placed in an aluminum pan, and a comparable weight of Al_2O_3 was used as a reference. The water content in each film was estimated on the basis of the weight loss up to 470 K by TGA. The films had similar thermal properties as the previous report (*37*). Then, the chemical composition was calculated by postulating that the feed ratios of CDP and SiO_2 particles to DNA were constant.

Dispersion state of SiO_2 particles in the composite films

The dispersion state of SiO_2 particles in a film state was examined by optical microscopy (VH-Z450, KEYENCE, Osaka, Japan) at room temperature. The sample was prepared by the solvent casting method from mixtures on freshly cleaved mica disks.

Filler network in the composite films

The γ dependence of the G^* for the films was examined using a rheometer (ARES-G2, TA Instruments, New Castle, DE, USA) at

an angular frequency of 6.28 rad s^{-1} and 298 K. The measurements were carried out with a sample diameter of 8 mm under an axial force of 30 g for sufficient contact with the sample space, which was surrounded by water droplet to prevent the sample from drying. The tensile behaviors of the DC films were recorded using a standard tensile testing machine TENSILON RTC1250 (A&D Company, Tokyo, Japan). The measurements were carried out at a relative humidity around 40% at room temperature with a crosshead speed of 10 mm min^{-1}.

SUPPLEMENTARY MATERIALS

Supplementary material for this article is available at https://science.org/doi/10.1126/sciadv.abn6349

REFERENCES AND NOTES

1. J. J. B. Cockburn, N. G. A. Abrescia, J. M. Grimes, G. C. Sutton, J. M. Diprose, J. M. Benevides, G. J. Thomas Jr., J. K. H. Bamford, D. H. Bamford, D. I. Stuart, Membrane structure and interactions with protein and DNA in bacteriophage PRD1. *Nature* **432**, 122–125 (2004).
2. K. S. Ramamurthi, S. Lecuyer, H. A. Stone, R. Losick, Geometric cue for protein localization in a bacterium. *Science* **323**, 1354–1357 (2009).
3. P. M. Llopis, A. F. Jackson, O. Sliusarenko, I. Surovtsev, J. Heinritz, T. Emonet, C. Jacobs-Wagner, Spatial organization of the flow of genetic information in bacteria. *Nature* **466**, 77–81 (2010).
4. T. Katayama, M. K. Nobu, H. Kusada, X.-Y. Meng, N. Hosogi, K. Uematsu, H. Yoshioka, Y. Kamagata, H. Tamaki, Isolation of a member of the candidate phylum 'Atribacteria' reveals a unique cell membrane structure. *Nat. Commun.* **11**, 6381 (2020).
5. C. A. J. Hoeve, E. A. DiMarzio, P. Peyser, Adsorption of polymer molecules at low surface coverage. *J. Chem. Phys.* **42**, 2558–2563 (1965).
6. P. G. de Gennes, Polymer solutions near an interface. Adsorption and depletion layers. *Macromolecules* **14**, 1637–1644 (1981).
7. J. F. Douglas, H. E. Johnson, S. Granick, A simple kinetic model of polymer adsorption and desorption. *Science* **262**, 2010–2012 (1993).
8. S. Napolitano, M. Wübbenhorst, The lifetime of the deviations from bulk behaviour in polymers confined at the nanoscale. *Nat. Commun.* **2**, 260 (2011).
9. Y. Fujii, Z. Yang, J. Leach, H. Atarashi, K. Tanaka, O. K. C. Tsui, Affinity of polystyrene films to hydrogen-passivated silicon and its relevance to the T_g of the films. *Macromolecules* **42**, 7418–7422 (2009).
10. P. Gin, N. Jiang, C. Liang, T. Taniguchi, B. Akgun, S. K. Satija, M. K. Endoh, T. Koga, Revealed architectures of adsorbed polymer chains at solid-polymer melt interfaces. *Phys. Rev. Lett.* **109**, 265501 (2012).
11. D. S. Fryer, R. D. Peters, E. J. Kim, J. E. Tomaszewski, J. J. de Pablo, P. F. Nealey, C. C. White, W.-l. Wu, Dependence of the glass transition temperature of polymer films on interfacial energy and thickness. *Macromolecules* **34**, 5627–5634 (2001).
12. K. Tanaka, Y. Tateishi, Y. Okada, T. Nagamura, M. Doi, H. Morita, Interfacial mobility of polymers on inorganic solids. *J. Phys. Chem. B* **113**, 4571–4577 (2009).
13. A. Bansal, H. Yang, C. Li, K. Cho, B. C. Benicewicz, S. K. Kumar, L. S. Schadler, Quantitative equivalence between polymer nanocomposites and thin polymer films. *Nat. Mater.* **4**, 693–698 (2005).
14. A. C. Balazs, T. Emrick, T. P. Russell, Nanoparticle polymer composites: Where two small worlds meet. *Science* **314**, 1107–1110 (2006).
15. A. K. Mohanty, S. Vivekanandhan, J.-M. Pin, M. Misra, Composites from renewable and sustainable resources: Challenges and innovations. *Science* **362**, 536–542 (2018).
16. C. Kim, A. Facchetti, T. J. Marks, Polymer gate dielectric surface viscoelasticity modulates pentacene transistor performance. *Science* **318**, 76–80 (2007).
17. J. M. H. M. Scheutjens, G. J. Fleer, Statistical theory of the adsorption of interacting chain molecules. 2. Train, loop, and tail size distribution. *J. Phys. Chem.* **84**, 178–190 (1980).
18. H.-P. Hsu, K. Binder, Effect of chain stiffness on the adsorption transition of polymers. *Macromolecules* **46**, 2496–2515 (2013).
19. Z. Chen, Investigating buried polymer interfaces using sum frequency generation vibrational spectroscopy. *Prog. Polym. Sci.* **35**, 1376–1402 (2010).
20. B. Zuo, H. Zhou, M. J. B. Davis, X. Wang, R. D. Priestley, Effect of local chain conformation in adsorbed nanolayers on confined polymer molecular mobility. *Phys. Rev. Lett.* **122**, 217801 (2019).
21. F. Sanger, A. R. Coulson, G. F. Hong, D. F. Hill, G. B. Petersen, Nucleotide sequence of bacteriophage λ DNA. *J. Mol. Biol.* **162**, 729–773 (1982).
22. W. Saenger, Polymorphism of DNA versus structural conservatism of RNA: Classification of A-, B-, and Z-type double helices, in *Principles of Nucleic Acid Structure* (Springer, 1984), pp. 220–241.
23. R. R. Netz, H. Orland, Variational charge renormalization in charged systems. *Eur. Phys. J. E Soft Matter* **11**, 301–311 (2003).
24. M. Rubinstein, R. H. Colby, Worm-like chain model, in *Polymer Physics* (Oxford Univ. Press, 2003), pp. 57–59.
25. C. Leung, A. Bestembayeva, R. Thorogate, J. Stinson, A. Pyne, C. Marcovich, J. Yang, U. Drechsler, M. Despont, T. Jankowski, M. Tschöpe, B. W. Hoogenboom, Atomic force microscopy with nanoscale cantilevers resolves different structural conformations of the DNA double helix. *Nano Lett.* **12**, 3846–3850 (2012).
26. S. Ido, K. Kimura, N. Oyabu, K. Kobayashi, M. Tsukada, K. Matsushige, H. Yamada, Beyond the helix pitch: Direct visualization of native DNA in aqueous solution. *ACS Nano* **7**, 1817–1822 (2013).
27. H. Kominami, K. Kobayashi, H. Yamada, Molecular-scale visualization and surface charge density measurement of Z-DNA in aqueous solution. *Sci. Rep.* **9**, 6851 (2019).
28. S. Ido, H. Kimiya, K. Kobayashi, H. Kominami, K. Matsushige, H. Yamada, Immunoactive two-dimensional self-assembly of monoclonal antibodies in aqueous solution revealed by atomic force microscopy. *Nat. Mater.* **13**, 264–270 (2014).
29. G. Binnig, C. F. Quate, C. Gerber, Atomic force microscope. *Phys. Rev. Lett.* **56**, 930–933 (1986).
30. D. Welch, M. P. Lettinga, M. Ripoll, Z. Dogic, G. A. Vliegenthart, Trains, tails and loops of partially adsorbed semi-flexible filaments. *Soft Matter* **11**, 7507–7514 (2015).
31. H. G. Hansma, D. E. Laney, DNA binding to mica correlates with cationic radius: Assay by atomic force microscopy. *Biophys. J.* **70**, 1933–1939 (1996).
32. G. Beaucage, S. Rane, S. Sukumaran, M. M. Satkowski, L. A. Schechtman, Y. Doi, Persistence length of isotactic poly(hydroxy butyrate). *Macromolecules* **30**, 4158–4162 (1997).
33. D. Nykypanchuk, M. M. Maye, D. van der Lelie, O. Gang, DNA-guided crystallization of colloidal nanoparticles. *Nature* **451**, 549–552 (2008).
34. M. Kroon, W. L. Vos, G. H. Wegdam, Structure and formation of a gel of colloidal disks. *Phys. Rev. E* **57**, 1962–1970 (1998).
35. Z. Hao, A. Ghanekarade, N. Zhu, K. Randazzo, D. Kawaguchi, K. Tanaka, X. Wang, D. S. Simmons, R. D. Priestley, B. Zuo, Mobility gradients yield rubbery surfaces on top of polymer glasses. *Nature* **596**, 372–376 (2021).
36. M. Modarresi, A. Mehandzhiyski, M. Fahlman, K. Tybrandt, I. Zozoulenko, Microscopic understanding of the granular structure and the swelling of PEDOT:PSS. *Macromolecules* **53**, 6267–6278 (2020).
37. Y. Morimitsu, H. Matsuno, N. Ohta, H. Sekiguchi, A. Takahara, K. Tanaka, Mechanical stabilization of deoxyribonucleic acid solid films based on hydrated ionic liquid. *Biomacromolecules* **21**, 464–471 (2020).
38. E. A. Strychalski, J. Geist, M. Gaitan, L. E. Locascio, S. M. Stavis, Quantitative measurements of the size scaling of linear and circular DNA in nanofluidic slitlike confinement. *Macromolecules* **45**, 1602–1611 (2012).
39. P.-k. Lin, C.-C. Hsieh, Y.-L. Chen, C.-F. Chou, Effects of topology and ionic strength on double-stranded DNA confined in nanoslits. *Macromolecules* **45**, 2920–2927 (2012).
40. F. Vargas-Lara, S. M. Stavis, E. A. Strychalski, B. J. Nablo, J. Geist, F. W. Starre, J. F. Douglas, Dimensional reduction of duplex DNA under confinement to nanofluidic slits. *Soft Matter* **11**, 8273–8284 (2015).
41. P.-G. de Gennes, *Scaling Concepts in Polymer Physics* (Cornell Univ. Press, 1979).
42. N. Jiang, J. Wang, X. Di, J. Cheung, W. Zeng, M. K. Endoh, T. Koga, S. K. Satija, Nanoscale adsorbed structures as a robust approach for tailoring polymer film stability. *Soft Mater* **12**, 1801–1809 (2016).
43. G. D. Wignall, D. G. H. Ballard, J. Schelten, Measurements of persistence length and temperature dependence of the radius of gyration in bulk atactic polystyrene. *Eur. Polym. J.* **10**, 861–865 (1974).
44. Y. Oda, D. Kawaguchi, Y. Morimitsu, S. Yamamoto, K. Tanaka, Direct observation of morphological transition for an adsorbed single polymer chain. *Sci. Rep.* **10**, 20914 (2020).
45. D. Y. Yoon, P. J. Flory, Persistence vectors for polypropylene, polystyrene, and poly (methyl methacrylate) chains. *J. Polym. Sci.* **14**, 1425–1431 (1976).
46. A. R. Payne, A note on the conductivity and modulus of carbon black-loaded rubbers. *J. Appl. Polym. Sci.* **9**, 1073–1082 (1965).
47. S. Guilbaud, L. Salomé, N. Destainville, M. Manghi, C. Tardin, Dependence of DNA persistence length on ionic strength and ion type. *Phys. Rev. Lett.* **122**, 028102 (2019).
48. C. R. Harris, K. J. Millman, S. J. van der Walt, R. Gommers, P. Virtanen, D. Cournapeau, E. Wieser, J. Taylor, S. Berg, N. J. Smith, R. Kern, M. Picus, S. Hoyer, M. H. van Kerkwijk, M. Brett, A. Haldane, J. F. del Río, M. Wiebe, P. Peterson, P. Gérard-Marchant, K. Sheppard, T. Reddy, W. Weckesser, H. Abbasi, C. Gohlke, T. E. Oliphant, Array programming with NumPy. *Nature* **585**, 357–362 (2020).
49. G. Bradski, The OpenCV Library. *Dr. Dobb's J. Softw. Tools* **120**, 122–125 (2000).
50. E. Jones, T. Oliphant, P. Peterson, SciPy: Open Source Scientific Tools for Python, www.scipy.org/ [accessed 13 June 2019].
51. S. J. Marrink, H. J. Risselada, S. Yefimov, D. P. Tieleman, A. H. de Vries, The MARTINI force field: Coarse grained model for biomolecular simulations. *J. Phys. Chem. B* **111**, 7812–7824 (2007).

52. M. J. Stevens, Interfacial fracture between highly cross-linked polymer networks and a solid surface: Effect of interfacial bond density. *Macromolecules* **34**, 2710–2718 (2001).
53. S. Yang, J. Qu, An investigation of the tensile deformation and failure of an epoxy/Cu interface using coarse-grained molecular dynamics simulations. *Modelling Simul. Mater. Sci. Eng.* **22**, 065011 (2014).

Acknowledgments: We thank the Tanaka laboratory members for the discussions. **Funding:** This work was supported by the JST-Mirai Program (JPMJMI18A2) to K.T., JSPS KAKENHI Grant-in-Aid for Scientific Research (B) (grant no. JP20H02790) to K.T., JSPS KAKENHI Grant-in-Aid for Scientific Research (B) (grant no. JP18H02037) to H.M., and NEDO Moonshot R&D Program (grant no. JPNP18016) to H.M. **Author contributions:** Conceptualization: K.T. Data curation: H.M. and K.T. Formal analysis: Y.M., H.M., Y.O., S.Y., and K.T. Funding acquisition: H.M. and K.T. Investigation: Y.M., H.M., Y.O., S.Y., and K.T. Methodology: Y.M., H.M., and K.T. Project administration: K.T. Resources: H.M. and K.T. Software: Y.M. Supervision: K.T. Validation: Y.M., H.M., Y.O., S.Y., and K.T. Writing—original draft: Y.M., H.M., and S.Y. Writing—review and editing: K.T. **Competing interests:** The authors declare that they have no competing interests. **Data and materials availability:** All data needed to evaluate the conclusions in the paper are present in the paper and/or the Supplementary Materials.

Submitted 9 December 2021
Accepted 24 August 2022
Published 12 October 2022
10.1126/sciadv.abn6349